Cardiovirus leader proteins retarget RSK kinases toward alternative substrates to perturb nucleocytoplasmic traffic

Belén Lizcano-Perret[1], Cécile Lardinois[1], Fanny Wavreil[1], Philippe Hauchamps[2], Gaëtan Herinckx[3], Frédéric Sorgeloos[1], Didier Vertommen[3], Laurent Gatto[2] and Thomas Michiels[1*]

[1] VIRO unit, de Duve Institute, Université Catholique de Louvain, Brussels, 1200, Belgium
[2] CBIO unit, de Duve Institute, Université Catholique de Louvain, Brussels, 1200, Belgium
[3] PHOS unit and MASSPROT platform, de Duve Institute, Université Catholique de Louvain, Brussels, 1200, Belgium

[*]Correspondence: thomas.michiels@uclouvain.be

Summary

Proteins from unrelated pathogens, including some RNA or DNA viruses and bacteria can recruit and activate cellular p90-ribosomal protein S6 kinases (RSKs) through a common linear motif. Data suggested a model where pathogens' proteins act to dock the recruited RSKs toward specific substrates, which then act as effectors to the benefit of the pathogens. Using cardiovirus leader protein (L) as a paradigm, we show that pathogens' proteins can modify the spectrum of RSK substrates in infected cells. L triggers nucleocytoplasmic trafficking perturbation and phenylalanine-glycine (FG)-nucleoporin hyperphosphorylation in an RSK-dependent fashion. Biotin ligase experiments identified FG-nucleoporins as common partners of L and RSK in infected cells. Using cells expressing an analog-sensitive RSK2 mutant, we show that L triggers direct phosphorylation of NUP98 and NUP214 by RSK2 in infected cells. Our data therefore demonstrate a novel virulence mechanism where pathogens' proteins hijack and retarget cellular protein kinases of the RSK family.

Keywords: Linear motifs, p90 ribosomal S6 kinases, Picornavirus, leader protein, nucleoporins, nuclear pore complex, phosphorylation, virulence, innate immunity escape, nucleocytoplasmic traffic

Introduction

Proteins encoded by several unrelated pathogens, including RNA viruses, DNA viruses and bacteria, were recently shown to use a common short linear motif (D/E-D/E-V-F, referred to as DDVF hereafter)

to recruit members of the cellular p90-ribosomal S6 protein kinases (RSKs) family: RSK1, RSK2, RSK3 and RSK4 (Sorgeloos et al., 2022, Alexa et al., 2022). Interestingly, competition and cross-linking experiments, as well as crystallography data show that these pathogens' proteins, the leader (L) protein (cardioviruses), ORF45 (Kaposi sarcoma-associated herpes virus - KSHV) and YopM (*Yersinia*) use a common interface to recruit RSKs. Binding of the pathogens' proteins prevents RSK dephosphorylation by cellular phosphatases, thereby maintaining RSK in an active state (Sorgeloos et al., 2022, Alexa et al., 2022). Although infection with all three pathogens leads to RSK activation, the outcome of this activation differs according to the protein bound to RSK. YopM association with RSK was proposed to inhibit the inflammasome and to lead to IL-10 production (Chung et al., 2016, Ratner et al., 2016); RSK recruitment by ORF45 enhances lytic replication of KSHV (Kuang et al., 2011, Li et al., 2015), whereas RSK recruitment by cardiovirus L protein leads to the inhibition of the antiviral eukaryotic initiation factor 2 alpha kinase 2 (EIF2AK2), better known as PKR (Sorgeloos et al., 2022). PKR inhibition by L was shown to depend on L interaction with RSK but also on L protein's C-terminal domain. Indeed, the M60V mutation in the C-terminal domain of L does not affect RSK recruitment but abolishes PKR inhibition. These observations led us to propose the "model of the clamp" whereby pathogens' proteins would act as adaptor proteins that force a given enzyme (here RSKs) to act on a specific substrate. Through their DDVF motif, pathogens' proteins recruit and maintain RSKs in an activated state. Through another domain (i.e. the C-terminal domain for L), they recruit proteins that could serve as substrate for RSKs. After phosphorylation, such proteins would act as effectors to the benefit of the pathogen (Figure 1A) (Sorgeloos et al., 2022). In an alternative model, proteins interacting with RSK through the conserved DDVF motif could directly act as preferential substrates for RSK-mediated phosphorylation (Figure 1B), as was suggested for protein RHBDF1 (Rhomboid 5 homolog 1) (Alexa et al., 2022).

Cardioviruses belong to the *Picornaviridae* family and include encephalomyocarditis virus (EMCV), Theiler's murine encephalomyelitis virus (TMEV) and the human Saffold virus (SAFV), closely related to TMEV. Despite its very small size (67-76 amino acids) and lack of enzymatic activity, the L protein encoded by these viruses was shown to be multifunctional as, beside inhibiting PKR, it blocks interferon gene transcription, and triggers an extensive diffusion of nuclear and cytoplasmic proteins across the nuclear membrane (Freundt et al., 2018, Brahic et al., 2005, van Pesch et al., 2001, Zoll et al., 2002, Hato et al., 2007, Borghese and Michiels, 2011, Borghese et al., 2019, Delhaye et al., 2004, Lidsky et al., 2006, Lizcano-Perret and Michiels, 2021, Sorgeloos et al., 2022). This nucleocytoplasmic trafficking perturbation was associated with the hyperphosphorylation of phenylalanine-glycine-nucleoporins (FG-NUPs) such as NUP98, NUP153 or NUP62 (Porter and Palmenberg, 2009, Porter et al., 2010, Ricour et al., 2009b, Bardina et al., 2009). FG-NUPs are proteins of the nuclear pore complex (NPC) that possess intrinsically disordered domains, rich in phenylalanine and glycine residues. These domains form a mesh in the center of the nuclear pore, which enables interaction with karyopherins, thus allowing selective transport of proteins and RNA through the NPC (Aramburu and Lemke, 2017,

Beck and Hurt, 2017, Hampoelz et al., 2019, Hülsmann et al., 2012). Molecular dynamic simulations predict that FG-NUP phosphorylation drastically decreases the density of FG-NUPs inside the pore (Mishra et al., 2019). Accordingly, electron microscopy analysis of EMCV-infected cells displayed such a density loss in the center of the NPC (Bardina et al., 2009). Through perturbation of the NPC, cardioviruses trigger a diffusion of nuclear proteins to the cytoplasm which can be used by the virus for viral replication and translation (Lizcano-Perret and Michiels, 2021).

Preliminary data suggested that nucleocytoplasmic trafficking perturbation by cardiovirus L proteins depended on RSK and on the recruitment of a cellular target by the L-RSK complex (model of the clamp). The aim of this work was to assess whether RSK could indeed be retargeted by L to a new substrate in infected cells and to identify such a substrate that could trigger nucleocytoplasmic trafficking perturbation. Our data show that L can recruit both RSK and FG-NUPs and that FG-NUPs can act as direct RSK substrates in infected cells. This work provides strong support to the model of the clamp and elucidates a novel virulence mechanism.

Results

Cardiovirus L-mediated nucleocytoplasmic trafficking perturbation depends on RSK recruitment by L

We tested whether L-mediated redistribution of nuclear and cytoplasmic proteins across the nuclear envelope and the hyperphosphorylation of FG-NUPs depends on both RSK and L. In agreement with previous reports (Delhaye et al., 2004), cytosolic diffusion of the nuclear protein PTB occurred in HeLa cells infected for 10 hours with TMEV expressing a wild type L protein (L^{WT}) but not in non-infected cells or in cells infected with viruses carrying the M60V mutation in the C-terminal part of L (L^{M60V})(Figures 2A and S1A). In the latter cells, PTB however partly appeared in cytosolic punctae, likely corresponding to stress granules that were shown to form in the absence of PKR inhibition by L (Borghese and Michiels, 2011). Importantly, L^{WT}-mediated PTB diffusion was almost abrogated in RSK-deficient HeLa cells (HeLa-RSK-TKO). Viral replication was also decreased in the absence of RSK, in agreement with increased PKR activation in these cells. Interestingly, PTB diffusion was restored after transduction of HeLa-RSK-TKO cells with lentiviruses expressing any of the four human RSK isoforms (Figures 2A and S1B). Accordingly, NUP98 hyperphosphorylation was dramatically decreased in HeLa-RSK-TKO cells and restored in cells transduced to express any of the four RSK isoforms (Figure 2B). Similar observations were made in the case of EMCV as soon as 5 hours post-infection, although dependence on RSK was less pronounced (Figures 2C-D and S1C-D). Thus, PTB diffusion out of the nucleus and NUP98 hyperphosphorylation depend on both L and RSK.

In addition, TMEV and EMCV expressing L^{WT} but not mutant L proteins triggered an RSK-dependent disruption of nucleocytoplasmic trafficking of other proteins harboring canonical nuclear export (NES)

111 and import (NLS) sequences, as shown by diffusion of GFP-NES and RFP-NLS proteins in live cells
112 that stably express these proteins (Figures 2E-G and S1E). This observation demonstrates that
113 nucleocytoplasmic redistribution of proteins was not specific to PTB. Again, RSK dependence of
114 protein redistribution was slightly less prominent for EMCV than for TMEV.
115 Ectopic expression of TMEV L^{WT} but not the L^{F48A} mutant (affected in the RSK-binding motif) was
116 sufficient to trigger nucleocytoplasmic redistribution of proteins (Figures 2H-J). Also, expression of
117 L^{M60V} or YopM did not affect nucleocytoplasmic trafficking although these proteins can activate RSK
118 (Sorgeloos et al., 2022). Taken together, these data show that L-mediated nucleocytoplasmic trafficking
119 alteration does not dependent on virus replication per se or on the expression of other viral proteins and
120 requires both interaction with RSK and, at least for TMEV L, integrity of the C-terminal part of the
121 protein.
122
123 **Identifying RSK partners in TMEV-infected cells using BioID2**
124 According to the model of the clamp, TMEV L would recruit RSK through its central DDVF motif and
125 would recruit potential RSK substrates through its C-terminal domain. As suggested above, the M60V
126 mutation of L would prevent the recruitment of such a target, without affecting RSK binding.
127 In order to identify target proteins that are recruited by L as potential RSK targets, we used the modified
128 bacterial biotin ligase BioID2 (BioID) which, when fused to a protein of interest, allows promiscuous
129 biotinylation of proximal proteins in the cell (Kim et al., 2016).
130 A BioID-RSK2 (BioID-RSK) fusion was constructed and expressed in RSK1/2-deficient HeLa cells
131 (HeLa-RSK-DKO) by lentiviral transduction to identify RSK's potential partners during TMEV
132 infection (Figure 3A). After testing that the BioID-RSK construct was activated (i.e. phosphorylated)
133 in the presence of L in infected cells and able to rescue L activities such as L-mediated PKR inhibition
134 (Figure S2A), we performed biotinylation experiments in order to identify RSK partners in the context
135 of infected cells. HeLa BioID-RSK cells were infected with either L^{WT} or L^{M60V} viruses for 16 hours in
136 presence of biotin. Biotinylated proteins were pulled down using streptavidin beads and processed for
137 mass spectrometry analysis. Western blot detection of biotinylated proteins (Figure 3B) confirmed the
138 concentration of biotinylated proteins in the pulled down fraction and revealed the presence of a 100kDa
139 band specific to the L^{WT}-infected sample, suggesting that the L protein status indeed influenced target
140 biotinylation by the BioID-RSK fusion.
141
142 **Identifying L protein partners using BioID**
143 Several attempts to identify proteins that are recruited by TMEV L were made in our lab by
144 coimmunoprecipitation. However, beside RSK, no clear L partner was consistently identified. It is not
145 unlikely that proteins recruited by L would interact with L only transiently and with low affinity. We
146 thus used the BioID system to identify such proteins that may transiently interact with L in infected
147 cells and then serve as RSK substrates. However, due to packaging limitations in picornaviruses, the

148 BioID coding sequence (696 nt) would be too long to be accommodated into the viral genome. We thus
149 generated *trans*-encapsidated replicons where a sequence coding for BioID-L and eGFP was substituted
150 for the capsid-coding region (Figure S2B). These replicons were encapsidated in 293T cells stably
151 expressing a capsid coding sequence carrying synonymous mutations in the VP2 region that affect *CRE*
152 function (Lobert et al., 1999) to prevents the selection of replication-competent wild type viruses that
153 might emerge through recombination. *Trans*-encapsidated replicons coding for BioID fused to L^{WT} ,
154 L^{M60V} and L^{F48A} were produced (Figure 3A). In HeLa cells infected with these replicons, L activities
155 (i.e. RSK phosphorylation, PKR activation and NUP98 hyperphosphorylation) were as expected (Figure
156 S2C). HeLa cells were then infected with BioID-L replicons for 14 hours in presence of biotin.
157 Biotinylated proteins were pulled down in stringent conditions. Western blot confirmed protein
158 biotinylation in infected cell extracts and showed some bands occurring in L^{WT} and L^{F48A} but not in
159 L^{M60V} samples (Figure 3C). These results confirm specific biotinylation of proteins by BioID-L.
160
161 **FG-NUPs are enriched in BioID-L and BioID-RSK proxeomes**
162 We expected that RSK targets recruited by L would be present in both BioID-RSK and BioID-L screens.
163 Pulled down biotinylated proteins from both screens (n=3 for each screen) were identified by mass
164 spectrometry (MS) and sorted according to their peptide spectrum match (PSM) number (for more detail
165 on the calculations see material and methods). For BioID-RSK, proteins were sorted according to their
166 abundance in L^{WT}-infected cells relative to that in non-infected cells and in cells infected with the L^{M60V}
167 mutant virus (Figure 3D, vertical axis). For BioID-L (replicons), proteins were sorted according to their
168 abundance in L^{WT} and L^{F48A} samples relative to that in L^{M60V}-infected and in non-infected samples
169 (Figure 3D, horizontal axis). Hence, the proteins that would be recruited by the C-terminal domain of
170 L are those that have high ratios in both screens. Interestingly, many of these proteins were FG-NUPs
171 (Figures 3D and E). ProDA (Probabilistic Dropout Analysis) statistical analysis (Ahlmann-Eltze and
172 Anders, 2020) was used to identify proteins whose abundance differs in pairwise comparisons: L^{WT}
173 versus L^{M60V} for the BioID-RSK experiments, and L^{WT} versus L^{M60V} or L^{F48A} versus L^{M60V} for the BioID-
174 L experiment. The table in Figure 3E shows adjusted P-values obtained from this analysis for the 20
175 best-ranked proteins. In the BioID-RSK experiments, FG-NUPs had the lowest adjusted P-values
176 (though not significant) and highest fold change (Figures 3E and F). In the BioID-L experiments many
177 FG-NUPs reached significant scores when pairwise comparisons were made between L^{WT} and L^{M60V} or
178 between L^{M60V} and L^{F48A} (Figures 3E and F). Most importantly, FG-NUPs that had previously been
179 shown to be hyperphosphorylated during cardiovirus infection: NUP62, NUP98, NUP153 and NUP214
180 (Porter and Palmenberg, 2009, Porter et al., 2010, Ricour et al., 2009b, Bardina et al., 2009) exhibited
181 statistical significance (Figure 3E). From these results we conclude that L recruits RSK through its
182 DDVF motif and then docks RSK toward FG-NUPs when the C-terminal domain of L is intact.
183
184 **Proteins biotinylated by BioID-RSK and BioID-L are localized at the NPC**

185 We analyzed the subcellular localization of proteins that were biotinylated by BioID-RSK and by
186 BioID-L in infected cells. To this end, biotinylation experiments were performed as above but infected
187 cells were fixed after 10h of infection, permeabilized and stained them with Alexa Fluor conjugated
188 streptavidin. For BioID-RSK, mock-infected cells show staining of biotinylated proteins in the nucleus,
189 in agreement with the mostly nuclear localization of RSKs (Chen et al., 1992) (Figures 4A-B and S3A).
190 In cells infected with the L^{WT} virus, biotinylated proteins form a faint rim around the nucleus, in addition
191 to the diffuse nuclear staining, showing that part of the (BioID-)RSK molecules are recruited to the
192 nuclear envelope. In cells infected with the L^{M60V} mutant virus, this nuclear rim is lost, in agreement
193 with a lack of L^{M60V} interaction with nucleoporins. For BioID-L replicons, staining occurs in the nucleus
194 and at the nuclear envelope for L^{WT}, in agreement with an interaction of L with both RSK and NUPs
195 (Figures 4C, D and S3B). Proteins biotinylated by BioID-L^{M60V} show diffuse staining in the nucleus, in
196 agreement with L^{M60V} interaction with RSK but not with nucleoporins. Proteins biotinylated by BioID-
197 L^{F48A} show extensive colocalization with nucleoporin POM121 at the nuclear envelope (Figure S3B),
198 in agreement with the lack of interaction with RSK, which would likely sequester part of the L protein
199 in the nucleoplasm. In conclusion, labeling of biotinylated proteins support our model where L interacts
200 with RSK in the nucleus and recruits a portion of RSK molecules to the NPC, via an interaction between
201 the C-terminal domain of L and NUPs.
202
203 **FG-NUPs are direct substrates for RSK in cardiovirus infected cells**
204 Since FG-NUPs are known to be hyperphosphorylated during cardiovirus infection and since our results
205 showed that RSK is in their close proximity, we aimed to test if RSK can directly phosphorylate these
206 FG-NUPs in infected cells. For this, we used the « analog-sensitive kinase system » developed by the
207 group of Shokat (Allen et al., 2007). This system is based on the use of an ATP analog: N6-alkylated
208 ATP-γ-S (A*TP-S), bulkier than ATP, that only fits in ATP binding pockets of kinases that have been
209 mutated to accommodate such bulkier analogs. The advantage of this technique is that the mutated
210 kinase (RSK in our case) is the only kinase in the cell that can use A*TP-S and will therefore
211 thiophosphorylate its substrates. After alkylation, such target proteins can be recognized using a specific
212 anti-thiophosphate ester antibody (Figure 5A). We identified Leu147 as the RSK2 "Gatekeeper" residue
213 (i.e. residue in the ATP-binding pocket that, when mutated to a smaller residue, allows the access of the
214 A*TP-S) by homology to Thr338 in the consensus sequence defined for c-SRC (Lopez et al., 2014)
215 (Figure S4A). Leu147 was mutated either to Gly (As1-RSK) or to Ala (As2-RSK). To test for ATP
216 analog usage by the modified RSK kinases, WT, As1- and As2-RSKs were stably expressed in HeLa-
217 RSK-TKO cells by lentiviral transduction, yielding WT-, As1- and As2-RSK cells. Expression of both
218 As1- and As2-RSK allowed L functions (i.e. PKR inhibition, RSK activation and NUP98
219 hyperphosphorylation)(Figure S4B). The ATP analog N6-Bn-ATP-γ-S was better incorporated than
220 N6-PhEt-ATP-γ-S by the As-RSKs (Figure S4C). The As2-RSK kinase was better expressed than As1-

221 RSK and readily accommodated this analog (Figures S4B and C). Therefore, As2-RSK cells and N6-
222 Bn-ATP-γ-S were chosen for further experiments. HeLa WT-RSK or As2-RSK cells were then infected
223 with L^{WT} and L^{M60V} viruses for 8h30min. Cells were then permeabilized with digitonin and treated with
224 A*TP-S (N6-Bn-ATP-γ-S) for 1 hour. Then, NUP98 was immunoprecipitated and its
225 thiophosphorylation status was analyzed, after alkylation, by western blot with the anti-thiophosphate
226 ester antibody. The blot shown in Figure 5B shows a band highly enriched in the immunoprecipitated
227 sample, migrating at the expected molecular mass for NUP98 (98kDa). This band was most prominent
228 in the samples from as2-RSK cells, confirming the specificity of thiophosphate ester detection.
229 Importantly, this band was detected much more in samples of cells infected with the L^{WT} virus than in
230 samples of cells that were not infected or infected with the L^{M60V} virus. These data indicate that NUP98
231 can be directly phosphorylated by RSK and, as expected, that this phosphorylation only occurs after
232 infection with the L^{WT} virus. For EMCV, as this virus replicates much faster than TMEV, NUP98 was
233 immunoprecipitated after 3h30 of infection. Thiophosphorylation of immunoprecipitated proteins was
234 tested by western blot using the anti-thiophosphate ester antibody (Figure 5C). As for TMEV, a
235 ~100kDa protein likely corresponding to NUP98 was thiophosphorylated by As2-RSK only in L^{WT}
236 infected conditions. It is noteworthy that additional bands were detected, which likely correspond to
237 other FG-NUPs such as NUP62, NUP153 and NUP214 that coimmunoprecipitated with NUP98.
238 In order to confirm FG-NUPs thiophosphorylation by As2-RSK in infected cells, experiments were
239 performed the other way around. Therefore, thiophosphorylated proteins were immunoprecipitated
240 from cells infected with TMEV variants, using the thiophosphate ester antibody. Then the IP fraction
241 (i.e. thiophosphorylated proteins) was analyzed by western blot for the presence of NUP98 (Figure 5D)
242 and NUP214 (Figure S4D). Again, these NUPs were most prominently detected in the conditions where
243 the L protein was WT and RSK was mutated (As2-RSK). These data confirm that RSK directly
244 phosphorylates FG-NUPs when the L^{WT} protein is present.
245
246 Taken together, these results confirm that part of the cellular RSKs can be redirected to the nuclear pore
247 complex by the L protein, where RSKs phosphorylate FG-NUPs. By interacting with RSK through its
248 DDVF motif and with FG-NUPs through its C-terminal domain, L serves as a viral adapter protein to
249 modulate RSK's activity and redirects these kinases toward new substrates. thus supporting the model
250 of the clamp. Hyperphosphorylation of FG-NUPs by RSK likely triggers a global perturbation of
251 nucleocytoplasmic trafficking and may therefore facilitate cytoplasmic replication of cardioviruses.
252
253 **Discussion**
254
255 Recent work showed that some proteins expressed by unrelated viruses and bacteria hijack host RSK
256 kinases through a conserved DDVF linear motif that likely emerged in those proteins by convergent

257 evolution (Sorgeloos et al., 2022, Alexa et al., 2022). Occurrence of the DDVF motif in RHBDF1, a
258 known target of RSKs suggests that some proteins, either from pathogens or from the host cell, can
259 associate with RSK through the DDVF motif to promote their own phosphorylation by RSKs (Alexa et
260 al., 2022). In the case of TMEV L protein, a point mutation in the C-terminal domain of the protein
261 (L^{M60V}) abrogated L activities although this mutation affected neither L-RSK interaction nor RSK
262 activation by L (Ricour et al., 2009a, Sorgeloos et al., 2022). The phenotype of this mutant supported
263 the model of the clamp where the pathogens' protein would act to bridge RSK to specific substrates.
264 The two models are not mutually exclusive.
265 Our data show that L proteins from TMEV and EMCV indeed act by redirecting part of the cellular
266 RSK kinases toward the nuclear pore complex where RSKs directly phosphorylate FG-NUPs.
267 Bacteria of the genus *Yersinia* use a type III secretion system to inject Yop proteins into contacted
268 eukaryotic cells (Cornelis and Wolf-Watz, 1997). YopM was shown to interact with RSK through a C-
269 terminal DDVF motif (Sorgeloos et al., 2022) and with protein kinase PKNs through central leucin-rich
270 motifs. Formation of the tripartite (YopM-RSK-PKN) complex results in the phosphorylation and
271 activation of PKN, which requires active RSK (McDonald et al., 2003, Hentschke et al., 2010),
272 suggesting that RSK might also be redirected toward PKN as a specific substrate. This scenario is very
273 likely although direct phosphorylation of PKN by RSK was not formally proven.
274 Another question regarding the clamp model is whether the substrates to which RSKs are redirected by
275 the pathogens' proteins are physiological RSK substrates, the phosphorylation of which is increased by
276 their forced association with RSKs or whether they represent unconventional RSK substrates. From the
277 blots of analog-sensitive RSK experiments (Figures 5B-D and S4D), it appears that basal
278 thiophosphorylation of NUP98 or NUP214 might occur, even in non-infected cells that do not contain
279 the L protein. Also, given that the main binding site of pathogens' proteins is located in a surface-
280 exposed loop of RSK, relatively remote from the catalytic site, it is unlikely that this interaction can
281 modify the catalytic site enough to accommodate structurally divergent substrates. Thus, the role of the
282 bridging proteins is likely to increase the frequency of encounters between RSKs and specific
283 substrates, and possibly also to drive these kinases to specific subcellular locations.
284 Viruses of the *Picornaviridae* family disturb nucleocytoplasmic traffic, likely to recruit host nuclear
285 RNA-binding proteins to the cytoplasm of the infected cells, where their genome translation and
286 replication takes place. Perturbation of the traffic was also reported to inhibit the activation of innate
287 immunity genes such as genes coding for interferon or chemokines, because these genes rely on the
288 translocation of transcription factors like IRF3/7 or NFκB (Lizcano-Perret and Michiels, 2021, De
289 Jesús-González et al., 2021). Enteroviruses encode proteases $2A^{pro}$ and $3C^{pro}$, which directly cleave FG-
290 NUPs (Saeed et al., 2020), thereby opening the central channel of the nuclear pore complex (Belov et
291 al., 2004, Bardina et al., 2009). Cardioviruses, however, induce the hyperphosphorylation of FG-NUPs,
292 thus mimicking a process occurring during mitosis, which ends up in the dismantling of the NPCs and
293 the free diffusion of nuclear and cytoplasmic proteins. Here, we show that TMEV L promotes direct

294 FG-NUPs phosphorylation by RSKs. During mitosis, FG-NUP phosphorylation was proposed to
295 involve mostly cyclin-dependent kinase 1 (CDK1), polo-like kinase 1 (PLK1) and NIMA-related
296 kinases (Linder et al., 2017, Hampoelz et al., 2019). A phosphoproteomic analysis by Kosako et al.
297 (Kosako et al., 2009) also suggested the involvement of the ERK pathway, ERK1/2 being the upstream
298 kinase of RSK. We hypothesize that RSKs might indeed contribute, to some extent, to NUP
299 phosphorylation during mitosis and that L triggers a stronger RSK-mediated FG-NUP phosphorylation
300 during infection.
301 Our work illustrates a new virulence mechanism whereby pathogens' proteins not only activate but also
302 redirect host kinases toward specific substrates and decipher how cardioviruses trigger RSK-mediated
303 FG-NUP hyperphosphorylation to perturb nucleocytoplasmic trafficking in the host cell.
304
305 **Acknowledgments**
306 We are grateful to Melissa Drappier for suggesting the analog-sensitive kinase experiments. We are
307 much indebted to Kevan Shokat for quick support and detailed protocols concerning this great
308 technique.
309 We thank Frank J.M. van Kuppeveld for the gift of anti-EMCV capsid antibodies. We thank Stéphane
310 Messe for excellent technical assistance, Nicolas Dauguet for expert help in cell sorting, and Eric
311 Freundt and Frank J.M. van Kuppeveld for critical reading of this manuscript.
312
313 BLP and CL were the recipients of FRIA fellowship from the belgian FNRS. Work was supported by
314 the EOS joint programme of Fonds de la recherche scientifique-FNRS and Fonds wetenschappelijk
315 onderzoek-Vlaanderen-FWO (EOS ID: 30981113 and 40007527), Belgian fund for Scientific
316 Research (PDR T.0185.14), Loterie Nationale through support to the de Duve Institute and Actions
317 de Recherches Concertées (ARC).
318
319
320 **Author Contributions** https://www.cell.com/pb/assets/raw/shared/guidelines/CRediT-taxonomy.pdf
321 Conceptualization: B.L.P. and T.M.
322 Methodology: B.L.P, C.L., D.V., F.S. and T.M.
323 Software:
324 Validation:
325 Formal analysis: P.H., F.S., L.G.
326 Investigation: B.L.P, F.W., G.H., D.V. and T.M.
327 Resources:
328 Data curation:
329 Writing – original draft: B.L.P.

330 Writing – review & editing: B.L.P., D.V., F.S. and T.M.
331 Visualization:
332 Supervision: T.M.
333 Project administration: T.M.
334 Funding acquisition: T.M.
335
336 **Declaration of Interests**
337 The authors declare no conflicts of interests
338
339 **Figure legends**
340
341 **Figure 1. Pathogen's proteins hijack RSK kinases.**
342 (A) Indirect substrate recruitment - model of the clamp: a pathogen's protein acts as an adaptor protein,
343 which binds and activates RSK through its DDVF motif and recruits a target protein to be
344 phosphorylated by RSK through another domain. (B) Direct substrate recruitment. A pathogen's protein
345 interacts with RSK through its DDVF motif and is directly phosphorylated by RSK.
346
347 **Figure 2. Nucleocytoplasmic traffic perturbation induced by cardioviruses depends on both the**
348 **L protein and RSK kinases.**
349 (A-D) PTB diffusion out of the nucleus and hyperphosphorylation of NUP98 depend on both L and
350 RSK. Graphs showing the percentage of cells with PTB diffusion (mean ± SD), among cells infected
351 by TMEV (3D-positive) for 10h (A) or by EMCV (capsid-positive) for 5h (C). Counts: 25-50 infected
352 cells per experiment (n=4). **** denotes significant differences (One-way ANOVA, $p < 0.0001$)
353 between HeLa-RSK-TKO cells transduced with an empty vector (HeLa TKO) and cells re-expressing
354 indicated RSK isoforms, for L^{WT}-infected samples. (B and D) Western blots showing the RSK-
355 dependent hyperphosphorylation of NUP98 (shift upwards) or the inhibition of PKR activation induced
356 by TMEV (B) or EMCV (D). 3D or 2A were detected as control of infection, and ß-actin as loading
357 control. (E-G) Graphs and confocal microscopy pictures showing the quantification of RFP-NLS and
358 GFP-NES diffusion (mean ± SD) in live HeLa-LVX cells infected with TMEV for 10h (E-F) or EMCV
359 for 4h30. HeLa-LVX cells were either WT, or RSK-TKO cells transduced with an empty vector (HeLa-
360 TKO) or re-expressing RSK1. (G). Counts: 50 cells per experiment (n=4). ****: denotes significant
361 differences as above. Scale bar: 20µm
362 (H-J) Impact of L on nucleocytoplasmic traffic. HeLa-LVX cells transfected with an empty plasmid or
363 with plasmids expressing L^{WT}, L mutants or YopM. (H) Graph showing the percentage of cells with
364 GFP-NES and RFP-NLS diffusion (mean ± SD). Counts: 70±5 cells per experiment (n=6). One-way
365 ANOVA test was used to compare all samples to L^{WT}. (I) Confocal microscopy of HeLa-LVX cells

366 24hours post-transfection. Scale bar: 20µm. (J) Western blot of HeLa-LVX cells 24h post-transfection.
367 FLAG staining shows the expression of L proteins and YopM.
368
369 **Figure 3. BioID-RSK and BioID-L proxeomes identify FG-NUPs as targets recruited by the L-**
370 **RSK complex.**
371 (A) Cartoon showing the expected biotinylation by BioID-RSK or BioID-L fusion proteins of a target
372 recruited by the C-terminal domain of L. (B) Western blot of proteins biotinylated by BioID-RSK in
373 lysates and pulled down samples of TMEV infected cells. HeLa BioID-RSK cells were incubated for 2
374 days without biotin. Cells were then infected for 16h (MOI 2.5) with L^{WT} or L^{M60V} viruses in medium
375 containing 5µM biotin. Biotinylated proteins were pulled-down using streptavidin-magnetic beads. (C)
376 Western blot of proteins biotinylated by BioID-L in lysates and pulled down samples of TMEV infected
377 cells. HeLa cells were infected for 14h (MOI 2.5) with BioID-L^{WT}, BioID-L^{M60V} or BioID-L^{F48A}
378 replicons in medium containing 5µM biotin. Biotinylated proteins were then pulled-down using
379 streptavidin-magnetic beads. (D) Proteins identified in the proximity of BioID-RSK (y axis) and BioID-
380 L (x axis). Y-axis shows proteins detected after infection with L^{WT} but not L^{M60V} viruses (=PSMs in
381 $L^{WT}/(L^{M60V}+NI+1)$). X-axis shows proteins detected after infection with BioID-L^{WT} or BioID-L^{F48A} but
382 not BioID-L^{M60V} replicons (= PSMs in $(L^{WT}+ L^{M60V})/(L^{F48A}+NI+1)$). FG-NUPs are identified by green
383 dots. (E) Table showing the adjusted P-values for the 20 best ranked proteins. Ranking was attributed
384 by multiplying the BioID-RSK ratio by the BioID-L ratio. Statistical analysis of pairwise comparisons
385 made between L^{WT} and L^{M60V} for BioID-RSK and between L^{WT} and L^{M60V} or L^{F48A} and L^{M60V} for BioID-
386 L. Adjusted P-values < 0.05 are colored in red, FG-NUPs are colored in green. (F) Volcano plots
387 showing the same pairwise comparisons as in E. Proteins having an adjusted P-value < 0.05 and a Log_2
388 fold change (LFC) > 1 are colored in red (= proteins in Q2). FG-NUPs are colored in green.
389
390 **Figure 4. Subcellular localization of proteins biotinylated by BioID-RSK and BioID-L.**
391 (A) Confocal microscopy images of biotinylated proteins (green) and 3D viral polymerase (red)
392 detected in BioID-RSK expressing HeLa cells infected with L^{WT} or L^{M60V} viruses for 10h (MOI 5). (B)
393 Quantification of cells showing a visible nuclear rim of biotinylated proteins in HeLa BioID-RSK cells
394 infected with L^{WT} or L^{M60V} viruses (mean ± SD). Counts: 42 ± 10 infected cells per experiment (n=4).
395 (C) Confocal microscopy images of biotinylated proteins stained with streptavidin-Alexa Fluor 594
396 (orange) and 3D viral polymerase (green) in HeLa cells infected for 10h with BioID-L^{WT}, BioID-L^{M60V}
397 or BioID-L^{F48A} replicons (MOI 5). (D) Quantification of nuclear rim staining in HeLa cells infected
398 with BioID-L^{WT}, BioID-L^{M60V} or BioID- L^{F48A} viruses (mean ± SD). Counts: 31 ± 11 infected cells per
399 experiment (n=4). 3D viral polymerase was stained as a control of infection. (A and C) White arrows
400 point to examples of cells exhibiting a nuclear rim staining. Scale bar: 10µm. (B and D) One-way
401 ANOVA tests were used to compare all samples with each other.
402

403 **Figure 5. RSK directly phosphorylates NUP98 and NUP214 in TMEV and EMCV infected cells.**
404 (A) Cartoon showing the principle of the analog-sensitive kinase system. The kinase mutated in the
405 ATP binding pocket (As-RSK) can use regular ATP as well as a bulkier ATP analog (A*TP-S). Use of
406 the ATP analog induces the thiophosphorylation of the substrate. After an alkylation reaction with
407 paranitrobenzylmesylate (PNBM), thiophosphates are converted to thiophosphate esters, which are
408 specifically recognized by an anti-thiophosphate ester antibody. All other wild-type kinases in the cell,
409 have normal ATP binding pockets that cannot accommodate the ATP analog. (B-D) HeLa cells
410 expressing As2-RSK or WT-RSK were infected with TMEV for 8h (MOI 5) (B and D) or with EMCV
411 for 3h30min (MOI 5) (C). Cells were then permeabilized with digitonin, and N6-Bn-ATP-γ-S was
412 added for 1 hour. Cells were then lysed and either NUP98 (B and D) or thio-phosphate-ester containing
413 proteins were immunoprecipitated (D). (B-C) Immunoblots showing a concentrated amount of NUP98
414 in the immunoprecipitation samples and thiophosphate-ester proteins. (D) Immunoblots showing
415 NUP98 in the thiophosphate ester IP fraction when L^{WT} is present. Detection of viral capsid in the
416 lysates was made as control for infection.
417
418 **STAR Methods**
419
420 **RESOURCE AVAILABILITY**
421
422 **Lead contact**
423 Further information and requests for resources and reagents should be directed to and will be fulfilled
424 by the lead contact, Thomas Michiels (thomas.michiels@uclouvain.be)
425
426 **Materials availability**
427 All reagents generated in this study are available upon request after completion of a Materials Transfer
428 Agreement
429
430 **Data and code availability**
431 The mass spectrometry proteomics data have been deposited to the ProteomeXchange Consortium via
432 the PRIDE partner repository with the dataset identifier PXD034604"..
433 MaxQuant outputs are available in the study repository https://github.com/UCLouvain-CBIO/2022-
434 RSK-Nups-VIRO
435 Codes: Processed data and reproducible proDA analyses scripts are available in the study repository at
436 https://github.com/UCLouvain-CBIO/2022-RSK-Nups-VIRO
437
438 **EXPERIMENTAL MODEL AND SUBJECT DETAILS**
439

440 **Cells**

441 The subclone of HeLa cells used in this work were HeLa M cells that reportedly have low endogenous
442 RNase L activity (kindly offered by R.H. Silvermann) (Dong et al., 2001).
443 HeLa-RSK-DKO, (RSK1- and RSK2-deficient) and HeLa-RSK-TKO (RSK-1, RSK2- and RSK3-
444 deficient) cells were obtained from HeLa M cells using the CRISPR-Cas9 technology (Sorgeloos et al.,
445 2022). As HeLa cells express very little RSK3 and virtually no RSK4 transcripts, both cell lines can be
446 considered as RSK-KO cells. One transcribed allele is however detected carrying a 81nt in-frame
447 deletion in RSK1 (Sorgeloos et al., 2022).
448 HeLa-LVX and HeLa-RSK-TKO-LVX were obtained by transduction of HeLa M cells and of HeLa-
449 RSK-TKO cells with pLVX-EF1alpha-2xGFP:NES-IRES-2xRFP:NLS. Clones showing regular
450 2xGFP:NES and 2xRFP:NLS expression levels under the fluorescent microscope were selected for
451 further use. HeLa BioID-RSK cells were obtained by transduction of HeLa-RSK-DKO cells with
452 BLP10 and transduced cell populations were then selected with 1mg/ml of G418 (Roche). BioID2-
453 RSK2 expression was then verified by western blot. HeLa WT-RSK, HeLa As1-RSK and HeLa As2-
454 RSK cells were obtained by transduction of HeLa-RSK-TKO cells with TM1117, BLP20 and BLP21
455 respectively and transduced cell populations were selected with 1mg/ml of G418 (Roche). WT, As1 or
456 As2-RSK expression was then tested by western blot.
457 HeLa-RSK-TKO cells were transduced with the empty lentiviral vector TM952 or with TM1116-19
458 derivatives expressing the four isoforms of human RSK. Transduced cell populations were selected
459 with 2mg/ml of G418.
460 BHK-CL13 and 293T-CL13 cells were obtained by lentiviral transduction of CL13 (TMEV capsid
461 precursor - IRES - mCherry) in the corresponding cells. mCherry-positive cells were then sorted by
462 FACS.
463 293T cells were kindly provided by F. Tangy (Pasteur Institute, Paris). Both HeLa M and 293T cells
464 and their derivatives were maintained in Dulbecco's modified Eagle medium (DMEM) (Lonza)
465 supplemented with 10% of fetal calf serum (FBS, Sigma), 100 U/ml penicillin and 100µg/ml
466 streptomycin (Thermo Fisher). BHK-21 cells (ATCC), used for viral production and titration, were
467 maintained in Glasgow's modified Eagle medium (GMEM) (Gibco) supplemented with 10% newborn
468 calf serum (Gibco), 100 U/ml penicillin, 100µg/ml streptomycin and 2.6g/l tryptose phosphate broth
469 (Difco). All cells were cultured at 37°C, in 5% CO2.
470

471 **Viruses**

472 TMEV viruses used in this study are derivatives of KJ6, a variant of the persistent DA strain (DA1
473 molecular clone) adapted to grow on L929 cells (Jnaoui and Michiels, 1998). FB09 carries the M60V
474 mutation in L (L^{M60V}), which was shown to abrogate L toxicity (Ricour et al., 2009a, Borghese and
475 Michiels, 2011). KJ6 and FB09 are indicated as TMEV L^{WT} and L^{M60V} respectively.

476 EMCV viruses used is this study are derived from pMC24, a Mengo virus molecular clone carrying a
477 shortened (24C) polyC tract (Duke and Palmenberg, 1989). The virus denoted EMCV^{WT} (used in Figure
478 5) is the virus produced from the pMC24 plasmid. Viruses denoted EMCV L^{WT} and L^{Zn} (used in Figure
479 1 and S1) are produced from plasmids pFS269 and pTM1098 and express N-terminally Flag-tagged L
480 proteins. L^{Zn} carries two point mutations (C19A and C22A) in the zinc finger of L, which likely affect
481 the overall structure of the protein (Cornilescu et al., 2008).
482 These viruses were produced by reverse genetics from plasmid constructions containing the full-length
483 viral cDNA sequences. To this end, BHK-21 cells were electroporated (1500V, 25µFd, no shunt
484 resistance) using a Gene pulser apparatus (Bio-Rad) with viral RNA produced by *in vitro* transcription
485 (RiboMax transcription kit P1300, Promega). Supernatants were collected 48-72h after electroporation,
486 when cytopathic effect was complete. After 2 to 3 freeze-thaw cycles, the supernatants containing the
487 virus were clarified by centrifugation at 1258g for 20 min and viruses were stored at -80°C. Viruses
488 were titrated by plaque assay in BHK-21 cells.
489
490 **Trans-encapsidated viral replicons**
491 FW12 is the replicon encoding for BioID2-HA-linker(3xGGGGS)-L^{WT}. This replicon derives from
492 TMEV DA1. It was constructed by replacing the capsid-coding region of the virus by a sequence coding
493 sequentially (5'-to-3'), in a single frame, for: BioID2-HA-linker(3xGGGGS)-L, the L/VP4 boundary
494 cleaved by protease 3C, eGFP, the VP2 coding segment encompassing the CRE sequence, the 3' end of
495 the 2A coding region and the following part of the viral genome (see Figure S2B). The BioID-L^{M60V}
496 (FW16) and BioID-L^{F48A} (FW17) viral replicons are derivates of FW12 carrying the indicated mutation.
497 Trans-encapsidation of the replicon occurred in 293T cells transduced with the lentiviral vector CL13
498 to stably express the viral capsid precursor protein. pCL13, the plasmid carrying the lentiviral vector,
499 is a pTM945 derivative expressing the 10 C-terminal aminoacids of L followed by the entire capsid
500 precursor of virus DA1. C-terminal residues of L were inserted in the construct to restore a genuine
501 L/VP4 clivage site for protease 3C, which allows the capsid protein to start with an N-terminal glycine,
502 potentially undergoing myristoylation (Chow et al., 1987). Importantly, 4 silent mutations were
503 introduced in the VP2 coding sequence corresponding to the *CRE* region to prevent the replication of
504 recombinant wild type viruses that would emerge through recombination between replicon RNA and
505 capsid-coding mRNA in packaging cells.
506 293T-CL13 cells were seeded (600,000/well) in 6-well plates. 24h after seeding, cells were transfected
507 (TransIT-mRNA, Mirus) with 5µg of replicon RNA previously obtained by *in vitro* transcription. Six
508 hours post-transfection, medium was changed to DMEM without serum. The infected cell population
509 was passaged 8 times and reseeded with part of the collected supernatant to amplify viral production.
510 Then, 150ml of replicon-containing supernatant was collected and filtered (0.45µm). SDS was then
511 added to a final concentration of 0.5% and, after 2h incubation at RT, supernatants were centrifuged for
512 5min, at 1258g at 20°C. Next, 13ml of clarified supernatant was added to a 2.6ml sucrose 30% cushion

513 in polyallomer tubes (Beckman) and centrifuged for 16h at 20°C, 25.000rpm in a SW28 swinging
514 bucket rotor. After ultracentrifugation, pellets containing the replicons were resuspended in 150µl of
515 10mM Tris-HCl pH 7.5. and further dialyzed in 10mM Tris-HCl pH 7.5. Replicons were then titrated
516 by plaque assay using BHK-21 cells stably expressing viral capsid proteins (BHK-21 CL13), and kept
517 at -80°C.
518
519 **Lentiviral vectors and cell transduction**
520 - pLVX-EF1alpha-2xGFP:NES-IRES-2xRFP:NLS was a gift from Fred Gage (Addgene plasmid #
521 71396) (Mertens et al., 2015)
522 Other lentiviral vectors used for protein expression were derived from pCCLsin.PPT.hPGK.GFP.pre.
523 (Follenzi et al., 2000)
524 - TM945 is a $Prom_{CMV}$-MCS-IRES-mCherry construct (Hermant et al., 2013)
525 - TM952 is a $Prom_{CMV}$-MCS-IRES-neo construct (Cesaro et al., 2021)
526 - BLP10 is a TM952 derivative coding for BioID2-HA-linker(3xGGGS)-MuRSK2. Note that this
527 construct expresses murine RSK2, which differs from human RSK2 by a single amino acid.
528 - BLP20 is a TM952 derivative coding for As1-RSK2 (hu-RSK2 with Analog-sensitive kinase 1 (As1)
529 mutation (Leu 147 → Gly).
530 - BLP21 is a TM952 derivative coding for As2-RSK2 (hu-RSK2 with Analog-sensitive kinase 2 (As2)
531 mutation (Leu 147 → Ala).
532 - CL13 is a TM945 derivative expressing the 10 C-terminal aminoacids of L followed by the entire
533 capsid precursor of virus DA1.
534 - TM1116, TM1117, TM1118 and TM1119 are TM952 derivatives carrying the sequences coding for
535 3xHA-Human RSK1, RSK2, RSK3 and RSK4 respectively (Sorgeloos et al., 2022). They were
536 constructed using the Gateway technology (Invitrogen) from donor plasmids Hs.RPS6KA1,
537 Hs.RPS6KA2, Hs.RPS6KA3 and Hs.RPS6KA6 kindly provided by Dominic Esposito through the
538 Addgene collection (Addgene refs: 70573, 70575, 70577, and 70579, respectively)
539 Lentiviruses were produced in 293T cells by co-transfection of the following plasmid, using TransIT-
540 LT1 reagent (Mirus Bio): 2.5 µg of lentiviral vector, 0.75 µg of pMD2-VSV-G (VSV-glycoprotein),
541 1.125 µg of pMDLg/pRRE (Gag-Pol), and 0.625 µg of pRSV-Rev (Rev). DNA quantities are for
542 transfection of 1 well of a 6-well plate. Supernatants were typically collected 72h post transfection and
543 filtered (porosity: 0.45µM). For transduction, cells were typically seeded in a 24-well plate as of 5,000
544 - 10,000 cells/well and infected 1 or 2 times with 100µL of filtered lentivirus.
545
546 **METHOD DETAILS**
547
548 **Biotinylation experiments**

549 BioID-RSK : HeLa BioID-RSK cells were seeded in 6-well plates at a density of 90,000 cells per well.
550 Two 6-well plates were used per condition. 24h after seeding the cells, the medium was changed to
551 OptiMEM (Gibco) depleted from biotin (previously incubated with streptavidin beads for 2h at 4°C,
552 then filtered). Cells were kept in OptiMEM without biotin for 48h, then they were infected with 600µl
553 of virus per well at an MOI of 2.5. One hour post-infection 2ml/well of DMEM containing 5µM biotin
554 was added. Infection proceeded for 16h. For immunostaining: 1,000 HeLa BioID-RSK cells were
555 seeded in wells of a 96-well plate. 24h after seeding the cells, the medium was changed to OptiMEM
556 without biotin. Cells were then incubated without biotin for 48h, then they were infected with 50µL of
557 virus per well at an MOI of 5. One hour post-infection 150µL of DMEM containing 5µM biotin was
558 added. Infection proceeded for 10h.
559 BioID-L : HeLa cells were seeded in 6-well plates as of 160,000 cells per well. Two 6-well plates were
560 used per condition. 24h after seeding, the cells were infected with 600µl of BioID-L replicons at an
561 MOI of 2.5. One hour post-infection 2ml/well of DMEM containing 5µM biotin was added. Infection
562 proceeded for 14h. For immunostaining: 3,500 HeLa cells were seeded in wells of a 96-well plate. 24h
563 after seeding, the cells were infected with 50µL of virus per well at an MOI of 5. One hour post-infection
564 150µL of DMEM containing 5µM biotin was added. Infection proceeded for 10h.
565
566 **Streptavidin Pulldown**
567 Cells were washed with PBS 3 times and lysed with 200µL/well of stringent lysis buffer (50mM Tris-
568 HCl pH 7.6, 500mM NaCl, 0.4% SDS, 1mM DTT, 1 tablet of Pierce phosphatase/protease inhibitor
569 (Thermo Scientific) per 10ml of lysis buffer) for 15 min at room temperature (RT). Lysates were then
570 diluted twice by addition of 200µl/well of 50mM Tris-HCl pH7.6 and homogenized by 10 passages
571 through 21G needles. Lysates were then cleared by centrifugation at 12,000g for 10 min at RT.
572 Supernatants were then transferred to new tubes, 200µL (per condition) of protein A/G magnetic beads
573 (Pierce) were added to remove non-specific binding and incubated for 30 min at RT. Supernatants were
574 then transferred to a new tube and a sample of 160µL per condition was mixed with 80µL of 3x Laemmli
575 buffer (cell lysate control). The rest of the supernatant was incubated for 2h at RT with 260µL (per
576 condition) of Streptavidin magnetic beads (Pierce). Streptavidin beads were then washed once with 2%
577 SDS, and twice with "normal lysis buffer" (50mM Tris-HCl pH 7.5, 100mM NaCl, 2mM EDTA, 0.5%
578 NP40, 1 tablet of phosphatase/protease inhibitor (Thermo Scientific) per 10ml of lysis buffer) for 5 min
579 at RT. Beads were resuspended in 40µl of 1x Laemmli buffer and heated for 5min at 100°C to allow
580 protein's separation from the beads. Supernatants were then conserved at -20°C.
581
582 **Immunostaining**
583 Cells seeded in 96-well screenstar plates (Greiner, 655866) were fixed with PBS-4% PFA for 5 min at
584 RT. Cells were then permeabilized with PBS-0.2% Triton X-100 (ICN Biomedicals Inc.) for 5 min at
585 RT. Cells were then blocked with TNB blocking reagent (Perkin Elmer) for 1h at RT. Antibodies were

586 diluted in TNB blocking reagent: rabbit anti-TMEV 3D polymerase 1/1000 (rabbit, kindly provided by
587 M.Brahic), anti-2A 1/1200 (rabbit, home-made), anti-NUP98 (rat, N1038, Sigma) 1/400, anti-POM121
588 (rabbit, 15645-1-AP, Proteintech) 1/400 or anti-PTB (mouse, 324800, Invitrogen) 1/400; and added to
589 the cells and incubated for 1h at RT. Cells were then washed three times with PBS-0.1% Tween 20 for
590 5 min. Cells were then incubated with secondary antibodies (anti-rat Alexa Fluor 594, anti-rabbit Alexa
591 Fluor 488 or anti-rabbit Alexa Fluor 594, 1/800, anti-mouse Alexa Fluor 488 1/400) or streptavidin
592 (Alexa fluor 488 or Alexa fluor 594, 1/500) for 1h at RT. Finally, cells were washed 3 times with PBS-
593 0.1% Tween 20 and kept in PBS-Azide 0.02% until analysis. Fluorescence analysis was made with a
594 spinning disk confocal microscope (Zeiss) and adjustment of the images was performed using the Zen
595 image analysis software (Zeiss). Exposure time, image brightness and contrast were adjusted equally
596 within an experiment. For LVX cells (qualitative analysis), brightness and contrast were adjusted using
597 the automatic "best fit" setting of the the Zen software.
598
599 **Western blotting**
600 Proteins in Laemmli buffer were heated for 5 minutes at 100°C. They were then run in 8 or 10% tris-
601 glycine SDS polyacrylamide gels and then transferred to either polyvinylidenefluoride or nitrocellulose
602 membranes (only for Mab414 detection). Membranes were blocked with TBS-5% non-fat dry milk
603 (Regilait) or TBS-5% BSA (for streptavidin-HRP blots) for 1 hour at RT. Primary antibodies: anti-2A
604 (TMEV, rabbit home-made 1/4000), anti-Phospho-S380-RSK(rabbit, CST11989 – Cell signaling
605 technology, 1/5000), anti-PKR (rabbit, 18244-1-AP – Proteintech, 1/4000), anti-Phospho-T446-PKR
606 (rabbit, AB32036 – Abcam, 1/4000), anti-ß-actin (mouse, A5441 – Sigma, 1/10,000), anti-TMEV 3D
607 polymerase (rabbit, kindly provided by M.Brahic, 1/2000), anti-NUP98 (rat, N1038 – Sigma, 1/2000),
608 , anti-HA (mouse, MMS101P – Covance, 1/4000), anti-phospho-Akt-substrates: RxxS*/T* (phospho-
609 RSK substrates, rabbit, CST9614 – Cell signaling technology, 1/1000), anti-thio-P-ester (rabbit, NBP2-
610 67738 – Novusbio, 1/1000), anti-TMEV capsid (home-made, 1/2000), anti-FLAG M2 (mouse, Sigma,
611 F1804 1/5000) were diluted in blocking solution and were incubated with membranes over-night.
612 Membranes were then washed 3 times for 15min with TBS-0.1% Tween 20. Secondary antibodies (anti-
613 rabbit, anti-mouse or anti-rat coupled to HRP, Dako, 1/5000) or Streptavidin-HRP (Dako, 1/1000) were
614 then added for 1h at RT. Then, membranes were washed three times with TBS-0.1% Tween 20, once
615 with TBS and revelation was made with SuperSignal West chemiluminescence substrate (Pico or Dura,
616 Thermoscientific).
617
618 **Mass spectrometry**
619 Streptavidin pulldown samples were resolved using a 10% Tris-Glycine SDS gel run until 6mm
620 migration in the separating gel. Proteins were colored using PageBlue (Thermo Scientific, 24620). The
621 6mm bands containing whole proteins were cut into 3 different slices and trypsin digested. Peptides
622 were dissolved in solvent A (0.1% TFA in 2% ACN), directly loaded onto reversed-phase pre-column

623 (Acclaim PepMap 100, Thermo Scientific) and eluted in backflush mode. Peptide separation was
624 performed using a reversed-phase analytical column (Acclaim PepMap RSLC, 0.075 x 250 mm,Thermo
625 Scientific) with a linear gradient of 4%-27.5% solvent B (0.1% FA in 98% ACN) for 35 min, 27.5%-
626 40% solvent B for 5 min, 40%-95% solvent B for 5 min and holding at 95% for the last 5 min at a
627 constant flow rate of 300 nl/min on an EASY-nLC 1000 RSLC system. The peptides were analyzed by
628 an Orbitrap Fusion Lumos tribrid mass spectrometer (ThermoFisher Scientific). The peptides were
629 subjected to NSI source followed by tandem mass spectrometry (MS/MS) in Fusion Lumos coupled
630 online to the nano-LC. Intact peptides were detected in the Orbitrap at a resolution of 120,000. Peptides
631 were selected with the quadrupole for MS/MS using HCD setting at 35; ion fragments were detected in
632 the ion trap. A data-dependent procedure that alternated between one MS scan followed by MS/MS
633 scans was applied for 3 seconds for ions above a threshold ion count of 5.0E3 in the MS survey scan
634 with 30.0s dynamic exclusion. The electrospray voltage applied was 2.1 kV. MS1 spectra were obtained
635 with an AGC target of 4E5 ions and a maximum injection time of 50ms, and MS2 spectra were acquired
636 with an AGC target of 1E4 ions and a maximum injection set to 35ms. For MS scans, the m/z scan
637 range was 375 to 1800. The resulting MS/MS data was processed using Sequest HT search engine
638 within Proteome Discoverer 2.5 SP1 against a *Homo Sapiens* protein database obtained from Uniprot
639 (78 787 entries) and containing the sequences of viral proteins and BioID2-RSK. Trypsin was specified
640 as cleavage enzyme allowing up to 2 missed cleavages, 4 modifications per peptide and up to 5 charges.
641 Mass error was set to 10 ppm for precursor ions and 0.1 Da for fragment ions. Oxidation on Met
642 (+15.995 Da), phosphorylation on Ser, Thr and Tyr (+79.966 Da), conversion of Gln (-17.027 Da) or
643 Glu (- 18.011 Da) to pyro-Glu at the peptide N-term, biotinylation of Lys (+ 226.077) were considered
644 as variable modifications. False discovery rate (FDR) was assessed using Percolator and thresholds for
645 protein, peptide and modification site were specified at 1%.
646 PSM Ratio calculations were as followed:

647 $$BioID - RSK: \frac{PSM(L^{WT})}{PSM(L^{M60V}) + PSM(mock) + 1} \qquad BioID - L: \frac{PSM(L^{WT}) + PSM(L^{F48A})}{PSM(L^{M60V}) + PSM(mock) + 1}$$

648

649

650 **GST-S6 recombinant production and purification**

651 ER2566 electrocompetent bacteria were electroporated with pFS208 (plasmid coding for GST-S6) and
652 cultured in 10mL of TSB at 37°C O/N. Bacteria were then amplified at 37°C in 300mL of TSB until
653 DO600 reaches 1. At this point, we added IPTG at a final concentration of 0.2mM and let it at 37°C for
654 2 hours. Then bacteria were centrifugated at 6,000rpm 15min 4°C and resuspended in PBS, 1% Triton,
655 0.2mM PMSF, 2mM EDTA, 0.1% ß-mercaptoethanol. Bacteria were lysed with French press and
656 centrifuged at 21,000g for 20 min at 4°C. Supernatant containing soluble protein was then kept for
657 GST-pulldown. GST-pulldown was performed with agarose-glutathion beads. GST-S6 was eluted from

658 the beads with 50mM Tris-HCl pH8 – 10mM glutathion and then purified by dialysis with 25mM Hepes
659 buffer at 4°C.
660
661 ***In vitro* kinase assay**
662 293T cells were seeded (500,000 cells/well) in 6-well plates. 24h after seeding, cells were transfected
663 with TransIT-LT1 reagent (Mirus Bio) with 2.5 µg of plasmids pTM1117 (coding for WT-RSK2),
664 pBLP20 (coding for As1-RSK2) and pBLP21 (coding for As2-RSK2). 6 hours post-transfection, cells
665 were treated with 32nM PMA over-night. HA-RSKs were then immunoprecipitated with anti-HA
666 magnetic beads. Therefore, cells were washed once with PBS and lysed with 150µL of lysis buffer
667 (50mM Tris-HCl pH8, 100mM NaCl, 0.5% NP40, 2mM EDTA, 1 tablet of phosphatase/protease
668 inhibitor (Thermo Scientific) per 10ml of lysis buffer) for 15min at 4°C. Lysates were then
669 homogenized by 10 passages through 21G needles and cleared by centrifugation at 12,000g for 10min
670 at 4°C. Supernatants were then transferred to new tubes, 12,5µl (per condition) of protein A/G magnetic
671 beads (Pierce) were added to remove non-specific binding and incubated for 30 min at 4°C.
672 Supernatants were then transferred to a new tube and a sample of 20µl/ condition was mixed with 10µL
673 of 3x Laemmli buffer (cell lysate control). The rest of the supernatant was incubated with 12.5µl of
674 HA-magnetic beads (Pierce) for 2h at 4°C. Beads were then washed 3 times with lysis buffer for 5 min
675 at 4°C and resuspended in 30µl of TBS, 1mM PMSF, 1mM Na_3VO_4, 1 tablet of phosphatase/protease
676 inhibitor (Thermo Scientific) per 10ml.
677 For one *in vitro* kinase reaction we put: 2.5µg of GST-S6 (recombinant substrate), 10µL of kinase buffer
678 5x (125mM Hepes pH 7.5, 250mM NaCl, 100mM ß-glycerophosphate, 5mM DTT, 100mM $MgCl_2$,
679 500µM Na_3VO_4), 0.5 µL of 10mM ATP (Roth, HN35.1) or A*TP analogs (BioLog), and water to a
680 final volume of 30µL. To this we added 10µL of the immunoprecipitated RSK and incubated everything
681 at 30°C for 30 min with shacking. Following this, the samples were alkylated with PNBM (Abcam) at
682 a final concentration of 2.5mM for 2 hours at room temperature with shacking. Reaction was stopped
683 by the addition of Laemmli buffer 3x. Samples were then heated at 100°C for 5 min, separated from the
684 magnetic beads and kept at -20°C.
685
686 **Thiophosphorylation in permeabilized cells**
687 1.5 x10^6 HeLa-RSK-TKO TM1117(WT-RSK2) or BLP21 (As2-RSK2) cells were seeded in 10-cm
688 dishes, 1 10-cm dish per condition. The next day, cells were infected at an MOI of 5 for 8h30min (for
689 TMEV) and 3h30min (for EMCV). After that, cells were permeabilized with 500µL of the analog-
690 kinase buffer: 20mM Hepes pH 7.5, 100mM KOAc, 5mM NaOAc, 2mM $MgOAc_2$, 1mM EGTA,
691 20µg/ml digitonin, 10mM $MgCl_2$, 0.5mM DTT, 1x phosphatase inhibitor cocktail 2 (P5726, Merck),
692 1x cOmplete protease inhibitor (REF), 57µg/ml creatin kinase (Calbiochem 23895), 5mM Creatin
693 phosphate (Calbiochem, 2380), 0.1mM ATP, 0.1 mM N6-Bn-A*TP analog (BioLog), 3mM GTP (Roth,

694 K056.4) in order to get the ATP analog inside the cells and the thiophosphorylation reaction to happen.
695 Reaction proceeded for 1h at 37°C, 5% CO2 with the dishes on a rocking plate.
696
697 **Immunoprecipitation after thiophosphorylation reactions.**
698 NUP98 IP: cells were lysed by adding 500µL of 2x salty lysis buffer (100mM Tris-HCl pH8, 800mM
699 NaCl, 2% Triton X-100, 4mM EDTA, 2mM DTT, 1 tablet of phosphatase/protease inhibitor (Thermo
700 Scientific) per 10ml of lysis buffer) to the analog-kinase buffer for 15 min at 4°C. Lysates were diluted
701 4x by addition of 3ml of regular lysis buffer (50mM Tris-HCl pH8, 100mM NaCl, 0.5% NP40, 2mM
702 EDTA, 1 tablet of phosphatase/protease inhibitor (Thermo Scientific) per 10ml of lysis buffer). Lysates
703 were then homogenized by 10 passages through 21G needles and cleared by centrifugation at 12,000g
704 for 10min at 4°C. Supernatants were then transferred to new tubes, 30µL (per condition) of protein A/G
705 magnetic beads (Pierce) were added to remove non-specific binding and incubated for 30 min at 4°C.
706 Supernatants were then transferred to a new tube and a sample of 200µL/ condition was alkylated with
707 PNBM at a final concentration of 2.5mM for 2h at RT. Then alkylation reaction was stopped by addition
708 of 3x Laemmli buffer (cell lysate control). The rest of the supernatant was incubated O/N at 4°C with
709 8µg (per condition) of anti- NUP98 (rat, N1038 – Sigma). 62.5µl of A/G beads per condition were
710 added and incubated for 2h at 4°C. A/G beads were then washed three times with regular lysis buffer
711 for 5 min at 4°C. Beads were resuspended in 40µl of kinase buffer 1x. The IP samples were then
712 alkylated with PNBM at a final concentration of 2.5mM for 2h at RT. Alkylation reaction was stopped
713 by the addition of 3x Laemmli, and immunoprecipitated proteins were separated from the beads after
714 heating 5min at 100°C.
715 Thiophosphate ester IP: cells were lysed by adding 500µL of 2x lysis buffer (100mM Tris-HCl pH8,
716 200mM NaCl, 1% NP40, 40mM EDTA, 1 tablet of phosphatase/protease inhibitor (Thermo Scientific)
717 per 10ml of lysis buffer) for 15min at 4°C. Lysates were then homogenized by 10 passages through
718 21G needles and cleared by centrifugation at 12,000g for 10min at 4°C. Supernatants were then
719 alkylated with PNBM at a final concentration of 2.5mM for 1h30min at RT. As PNBM inhibits
720 immunoprecipitation, lysates were run through PD10 columns to remove PNBM prior to the
721 immunoprecipitation procedure. Fractions containing protein were kept and incubated with 30µl per
722 condition of A/G magnetic beads (to avoid non-specific binding) for 30 min at 4°C. Supernatants were
723 then transferred to a new tube and 1/10th of the lysate (200µl) was mixed with 100µl of 3x Laemmli
724 (cell lysate control). The rest of the supernatant was incubated with 8µg per condition of anti-
725 thiophosphate ester antibody (rabbit, NBP2-67738 – Novusbio) for 2h at 4°C. Then 62.5µl per condition
726 of A/G magnetic beads were added and incubated for 2h at 4°C. A/G beads were then washed three
727 times with regular lysis buffer for 5 min at 4°C and resuspended in 60µl of Laemmli 1x.
728 Immunoprecipitated proteins were separated from the beads after heating 5min at 100°C.
729
730 **QUANTIFICATION AND STATISTICAL ANALYSIS**

731

732 **Data processing and statistical analysis (for MS)**

733 Protein identification and label-free quantitation were performed with MaxQuant version
734 1.6.7.0.(Cox and Mann, 2008). Database searching was performed against the UniProt FASTA
735 database, using a false-discovery rate at the peptide and protein level was set to 0.01 and
736 allowing a maximum of two missed cleavages. All search parameters are available in the
737 parameter file available in the study repository (https://github.com/UCLouvain-CBIO/2022-
738 RSK-Nups-VIRO). After filtering out of identified contaminants, identified reverse sequences
739 and proteins having missing values in all samples, Max Quant protein intensities were log-2
740 transformed and normalized using sample median alignment. In order to cope with the
741 numerous drop-outs in protein intensities, the proDA method, as described in (Ahlmann-Eltze
742 and Anders, 2020) was applied.

743 For the analysis of the BioID-L experiment, the backbone linear model included one indicator
744 variable representing a potential batch effect between 2 groups of replicates, and 2 condition
745 indicator variables, representing the effect of resp. WT and F48A conditions with respect to
746 the reference condition, i.e. M60V condition. Potential batch effect was tested for each protein
747 using two-sided Wald test on the batch indicator variable. Since adjusted p-values were > 0.2
748 for all proteins, this indicator variable was subsequently removed from the model. Then, the
749 effects of WT and F48 conditions (w.r.t. M60V) were tested, for each protein, using one-sided
750 Wald tests, since the anticipated sign of the effect was known. All p-values were adjusted using
751 Benjamini-Hochberg corrections (Benjamini and Hochberg, 1995).

752 For the analysis of the BioID-RSK experiment, the backbone linear model included one
753 indicator variable representing a potential batch effect between 2 groups of replicates, and 1
754 condition indicator variable, representing the effect of WT condition with respect to the
755 reference condition, i.e. M60V condition. Potential batch effect was tested for each protein
756 using two-sided Wald test on the batch indicator variable. Since adjusted p-values were > 0.6
757 for all proteins, this indicator variable was subsequently removed from the model. Then, the
758 effect of WT condition (w.r.t. M60V) was tested, for each protein, using a one-sided Wald test,
759 since the anticipated sign of the effect was known. All p-values were adjusted using
760 Benjaminin-Hochberg corrections.

761

762 **Statistical analysis on IF**

763 Statistical analysis on immunofluorescence experiments was done using GraphPad Prism v9 A one-
764 way ANOVA test was used. The number of independent experiments (n) and statistical comparison
765 groups are indicated in the figures and figure legends.
766
767 **References**

768 AHLMANN-ELTZE, C. & ANDERS, S. 2020. proDA: Probabilistic Dropout Analysis for
769 Identifying Differentially Abundant Proteins in Label-Free Mass Spectrometry.
770 *bioRxiv*, 661496.
771 ALEXA, A., SOK, P., GROSS, F., ALBERT, K., KOBORI, E., PÓTI Á, L., GÓGL, G.,
772 BENTO, I., KUANG, E., TAYLOR, S. S., ZHU, F., CILIBERTO, A. & REMÉNYI,
773 A. 2022. A non-catalytic herpesviral protein reconfigures ERK-RSK signaling by
774 targeting kinase docking systems in the host. *Nat Commun,* 13**,** 472.
775 ALLEN, J. J., LI, M., BRINKWORTH, C. S., PAULSON, J. L., WANG, D., HÜBNER, A.,
776 CHOU, W. H., DAVIS, R. J., BURLINGAME, A. L., MESSING, R. O.,
777 KATAYAMA, C. D., HEDRICK, S. M. & SHOKAT, K. M. 2007. A semisynthetic
778 epitope for kinase substrates. *Nat Methods,* 4**,** 511-6.
779 ARAMBURU, I. V. & LEMKE, E. A. 2017. Floppy but not sloppy: Interaction mechanism of
780 FG-nucleoporins and nuclear transport receptors. *Semin Cell Dev Biol,* 68**,** 34-41.
781 BARDINA, M. V., LIDSKY, P. V., SHEVAL, E. V., FOMINYKH, K. V., VAN
782 KUPPEVELD, F. J., POLYAKOV, V. Y. & AGOL, V. I. 2009. Mengovirus-induced
783 rearrangement of the nuclear pore complex: hijacking cellular phosphorylation
784 machinery. *J Virol,* 83**,** 3150-61.
785 BECK, M. & HURT, E. 2017. The nuclear pore complex: understanding its function through
786 structural insight. *Nat Rev Mol Cell Biol,* 18**,** 73-89.
787 BELOV, G. A., LIDSKY, P. V., MIKITAS, O. V., EGGER, D., LUKYANOV, K. A., BIENZ,
788 K. & AGOL, V. I. 2004. Bidirectional increase in permeability of nuclear envelope
789 upon poliovirus infection and accompanying alterations of nuclear pores. *J Virol,* 78**,**
790 10166-77.
791 BENJAMINI, Y. & HOCHBERG, Y. 1995. Controlling the False Discovery Rate: A Practical
792 and Powerful Approach to Multiple Testing. *Journal of the Royal Statistical Society.*
793 *Series B (Methodological),* 57**,** 289-300.
794 BORGHESE, F. & MICHIELS, T. 2011. The leader protein of cardioviruses inhibits stress
795 granule assembly. *J Virol,* 85**,** 9614-22.
796 BORGHESE, F., SORGELOOS, F., CESARO, T. & MICHIELS, T. 2019. The Leader Protein
797 of Theiler's Virus Prevents the Activation of PKR. *J Virol,* 93.
798 BRAHIC, M., BUREAU, J. F. & MICHIELS, T. 2005. The genetics of the persistent infection
799 and demyelinating disease caused by Theiler's virus. *Annu Rev Microbiol,* 59**,** 279-98.
800 CESARO, T., HAYASHI, Y., BORGHESE, F., VERTOMMEN, D., WAVREIL, F. &
801 MICHIELS, T. 2021. PKR activity modulation by phosphomimetic mutations of serine
802 residues located three aminoacids upstream of double-stranded RNA binding motifs.
803 *Sci Rep,* 11**,** 9188.
804 CHEN, R. H., SARNECKI, C. & BLENIS, J. 1992. Nuclear localization and regulation of erk-
805 and rsk-encoded protein kinases. *Mol Cell Biol,* 12**,** 915-27.
806 CHOW, M., NEWMAN, J. F., FILMAN, D., HOGLE, J. M., ROWLANDS, D. J. & BROWN,
807 F. 1987. Myristylation of picornavirus capsid protein VP4 and its structural
808 significance. *Nature,* 327**,** 482-6.
809 CHUNG, L. K., PARK, Y. H., ZHENG, Y., BRODSKY, I. E., HEARING, P., KASTNER, D.
810 L., CHAE, J. J. & BLISKA, J. B. 2016. The Yersinia Virulence Factor YopM Hijacks

811 Host Kinases to Inhibit Type III Effector-Triggered Activation of the Pyrin
812 Inflammasome. *Cell Host Microbe,* 20**,** 296-306.
813 CORNELIS, G. R. & WOLF-WATZ, H. 1997. The Yersinia Yop virulon: a bacterial system
814 for subverting eukaryotic cells. *Mol Microbiol,* 23**,** 861-7.
815 CORNILESCU, C. C., PORTER, F. W., ZHAO, K. Q., PALMENBERG, A. C. & MARKLEY,
816 J. L. 2008. NMR structure of the mengovirus Leader protein zinc-finger domain. *FEBS*
817 *Lett,* 582**,** 896-900.
818 COX, J. & MANN, M. 2008. MaxQuant enables high peptide identification rates,
819 individualized p.p.b.-range mass accuracies and proteome-wide protein quantification.
820 *Nat Biotechnol,* 26**,** 1367-72.
821 DE JESÚS-GONZÁLEZ, L. A., PALACIOS-RÁPALO, S., REYES-RUIZ, J. M., OSUNA-
822 RAMOS, J. F., CORDERO-RIVERA, C. D., FARFAN-MORALES, C. N.,
823 GUTIÉRREZ-ESCOLANO, A. L. & DEL ÁNGEL, R. M. 2021. The Nuclear Pore
824 Complex Is a Key Target of Viral Proteases to Promote Viral Replication. *Viruses,* 13**,**
825 706.
826 DELHAYE, S., VAN PESCH, V. & MICHIELS, T. 2004. The leader protein of Theiler's virus
827 interferes with nucleocytoplasmic trafficking of cellular proteins. *J Virol,* 78**,** 4357-62.
828 DONG, B., NIWA, M., WALTER, P. & SILVERMAN, R. H. 2001. Basis for regulated RNA
829 cleavage by functional analysis of RNase L and Ire1p. *Rna,* 7**,** 361-73.
830 DUKE, G. M. & PALMENBERG, A. C. 1989. Cloning and synthesis of infectious cardiovirus
831 RNAs containing short, discrete poly(C) tracts. *J Virol,* 63**,** 1822-6.
832 FOLLENZI, A., AILLES, L. E., BAKOVIC, S., GEUNA, M. & NALDINI, L. 2000. Gene
833 transfer by lentiviral vectors is limited by nuclear translocation and rescued by HIV-1
834 pol sequences. *Nat Genet,* 25**,** 217-22.
835 FREUNDT, E. C., DRAPPIER, M. & MICHIELS, T. 2018. Innate Immune Detection of
836 Cardioviruses and Viral Disruption of Interferon Signaling. *Front Microbiol,* 9**,** 2448.
837 HAMPOELZ, B., ANDRES-PONS, A., KASTRITIS, P. & BECK, M. 2019. Structure and
838 Assembly of the Nuclear Pore Complex. *Annu Rev Biophys,* 48**,** 515-536.
839 HATO, S. V., RICOUR, C., SCHULTE, B. M., LANKE, K. H., DE BRUIJNI, M., ZOLL, J.,
840 MELCHERS, W. J., MICHIELS, T. & VAN KUPPEVELD, F. J. 2007. The
841 mengovirus leader protein blocks interferon-alpha/beta gene transcription and inhibits
842 activation of interferon regulatory factor 3. *Cell Microbiol,* 9**,** 2921-30.
843 HENTSCHKE, M., BERNEKING, L., BELMAR CAMPOS, C., BUCK, F.,
844 RUCKDESCHEL, K. & AEPFELBACHER, M. 2010. Yersinia virulence factor YopM
845 induces sustained RSK activation by interfering with dephosphorylation. *PLoS One,* 5.
846 HERMANT, P., FRANCIUS, C., CLOTMAN, F. & MICHIELS, T. 2013. IFN-ε is
847 constitutively expressed by cells of the reproductive tract and is inefficiently secreted
848 by fibroblasts and cell lines. *PLoS One,* 8**,** e71320.
849 HÜLSMANN, B. B., LABOKHA, A. A. & GÖRLICH, D. 2012. The permeability of
850 reconstituted nuclear pores provides direct evidence for the selective phase model. *Cell,*
851 150**,** 738-51.
852 JNAOUI, K. & MICHIELS, T. 1998. Adaptation of Theiler's virus to L929 cells: mutations in
853 the putative receptor binding site on the capsid map to neutralization sites and modulate
854 viral persistence. *Virology,* 244**,** 397-404.
855 KIM, D. I., JENSEN, S. C., NOBLE, K. A., KC, B., ROUX, K. H., MOTAMEDCHABOKI,
856 K. & ROUX, K. J. 2016. An improved smaller biotin ligase for BioID proximity
857 labeling. *Mol Biol Cell,* 27**,** 1188-96.
858 KOSAKO, H., YAMAGUCHI, N., ARANAMI, C., USHIYAMA, M., KOSE, S., IMAMOTO,
859 N., TANIGUCHI, H., NISHIDA, E. & HATTORI, S. 2009. Phosphoproteomics reveals

new ERK MAP kinase targets and links ERK to nucleoporin-mediated nuclear transport. *Nat Struct Mol Biol,* 16**,** 1026-35.

KUANG, E., FU, B., LIANG, Q., MYOUNG, J. & ZHU, F. 2011. Phosphorylation of eukaryotic translation initiation factor 4B (EIF4B) by open reading frame 45/p90 ribosomal S6 kinase (ORF45/RSK) signaling axis facilitates protein translation during Kaposi sarcoma-associated herpesvirus (KSHV) lytic replication. *J Biol Chem,* 286**,** 41171-41182.

LI, X., DU, S., AVEY, D., LI, Y., ZHU, F. & KUANG, E. 2015. ORF45-Mediated Prolonged c-Fos Accumulation Accelerates Viral Transcription during the Late Stage of Lytic Replication of Kaposi's Sarcoma-Associated Herpesvirus. *J Virol,* 89**,** 6895-906.

LIDSKY, P. V., HATO, S., BARDINA, M. V., AMINEV, A. G., PALMENBERG, A. C., SHEVAL, E. V., POLYAKOV, V. Y., VAN KUPPEVELD, F. J. & AGOL, V. I. 2006. Nucleocytoplasmic traffic disorder induced by cardioviruses. *J Virol,* 80**,** 2705-17.

LINDER, M. I., KÖHLER, M., BOERSEMA, P., WEBERRUSS, M., WANDKE, C., MARINO, J., ASHIONO, C., PICOTTI, P., ANTONIN, W. & KUTAY, U. 2017. Mitotic Disassembly of Nuclear Pore Complexes Involves CDK1- and PLK1-Mediated Phosphorylation of Key Interconnecting Nucleoporins. *Dev Cell,* 43**,** 141-156.e7.

LIZCANO-PERRET, B. & MICHIELS, T. 2021. Nucleocytoplasmic Trafficking Perturbation Induced by Picornaviruses. *Viruses,* 13**,** 1210.

LOBERT, P. E., ESCRIOU, N., RUELLE, J. & MICHIELS, T. 1999. A coding RNA sequence acts as a replication signal in cardioviruses. *Proc Natl Acad Sci U S A,* 96**,** 11560-5.

LOPEZ, M. S., KLIEGMAN, J. I. & SHOKAT, K. M. 2014. The logic and design of analog-sensitive kinases and their small molecule inhibitors. *Methods Enzymol,* 548**,** 189-213.

MCDONALD, C., VACRATSIS, P. O., BLISKA, J. B. & DIXON, J. E. 2003. The yersinia virulence factor YopM forms a novel protein complex with two cellular kinases. *J Biol Chem,* 278**,** 18514-23.

MERTENS, J., PAQUOLA, A. C. M., KU, M., HATCH, E., BÖHNKE, L., LADJEVARDI, S., MCGRATH, S., CAMPBELL, B., LEE, H., HERDY, J. R., GONÇALVES, J. T., TODA, T., KIM, Y., WINKLER, J., YAO, J., HETZER, M. W. & GAGE, F. H. 2015. Directly Reprogrammed Human Neurons Retain Aging-Associated Transcriptomic Signatures and Reveal Age-Related Nucleocytoplasmic Defects. *Cell Stem Cell,* 17**,** 705-718.

MISHRA, A., SIPMA, W., VEENHOFF, L. M., VAN DER GIESSEN, E. & ONCK, P. R. 2019. The Effect of FG-Nup Phosphorylation on NPC Selectivity: A One-Bead-Per-Amino-Acid Molecular Dynamics Study. *Int J Mol Sci,* 20.

PORTER, F. W., BROWN, B. & PALMENBERG, A. C. 2010. Nucleoporin phosphorylation triggered by the encephalomyocarditis virus leader protein is mediated by mitogen-activated protein kinases. *J Virol,* 84**,** 12538-48.

PORTER, F. W. & PALMENBERG, A. C. 2009. Leader-induced phosphorylation of nucleoporins correlates with nuclear trafficking inhibition by cardioviruses. *J Virol,* 83**,** 1941-51.

RATNER, D., ORNING, M. P., PROULX, M. K., WANG, D., GAVRILIN, M. A., WEWERS, M. D., ALNEMRI, E. S., JOHNSON, P. F., LEE, B., MECSAS, J., KAYAGAKI, N., GOGUEN, J. D. & LIEN, E. 2016. The Yersinia pestis Effector YopM Inhibits Pyrin Inflammasome Activation. *PLoS Pathog,* 12**,** e1006035.

RICOUR, C., BORGHESE, F., SORGELOOS, F., HATO, S. V., VAN KUPPEVELD, F. J. & MICHIELS, T. 2009a. Random mutagenesis defines a domain of Theiler's virus leader protein that is essential for antagonism of nucleocytoplasmic trafficking and cytokine gene expression. *J Virol,* 83**,** 11223-32.

RICOUR, C., DELHAYE, S., HATO, S. V., OLENYIK, T. D., MICHEL, B., VAN KUPPEVELD, F. J., GUSTIN, K. E. & MICHIELS, T. 2009b. Inhibition of mRNA export and dimerization of interferon regulatory factor 3 by Theiler's virus leader protein. *J Gen Virol,* 90**,** 177-86.

SAEED, M., KAPELL, S., HERTZ, N. T., WU, X., BELL, K., ASHBROOK, A. W., MARK, M. T., ZEBROSKI, H. A., NEAL, M. L., FLODSTRÖM-TULLBERG, M., MACDONALD, M. R., AITCHISON, J. D., MOLINA, H. & RICE, C. M. 2020. Defining the proteolytic landscape during enterovirus infection. *PLoS Pathog,* 16**,** e1008927.

SORGELOOS, F., PEETERS, M., HAYASHI, Y., BORGHESE, F., CAPELLI, N., DRAPPIER, M., CESARO, T., COLAU, D., STROOBANT, V., VERTOMMEN, D., DE BODT, G., MESSE, S., FORNÉ, I., MUELLER-PLANITZ, F., COLLET, J. F. & MICHIELS, T. 2022. A case of convergent evolution: Several viral and bacterial pathogens hijack RSK kinases through a common linear motif. *Proc Natl Acad Sci U S A,* 119.

VAN PESCH, V., VAN EYLL, O. & MICHIELS, T. 2001. The leader protein of Theiler's virus inhibits immediate-early alpha/beta interferon production. *J Virol,* 75**,** 7811-7.

ZOLL, J., MELCHERS, W. J., GALAMA, J. M. & VAN KUPPEVELD, F. J. 2002. The mengovirus leader protein suppresses alpha/beta interferon production by inhibition of the iron/ferritin-mediated activation of NF-kappa B. *J Virol,* 76**,** 9664-72.

Figure 1.

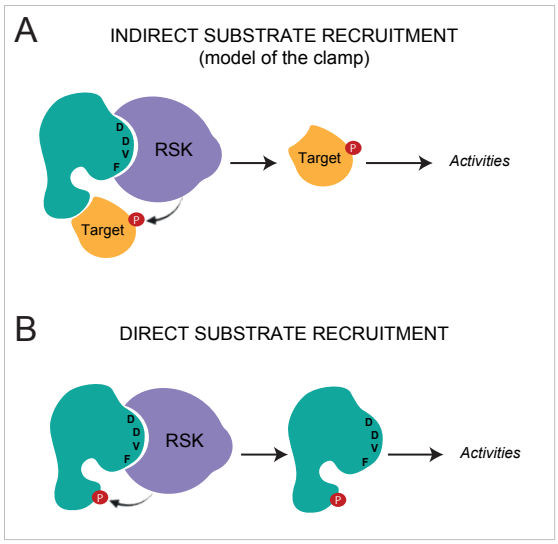
A
INDIRECT SUBSTRATE RECRUITMENT
(model of the clamp)
D
D
V
F
RSK
Target
P
Target
P
Activities
B
DIRECT SUBSTRATE RECRUITMENT
D
D
V
F
RSK
P
D
D
V
F
P
Activities

Figure 2.

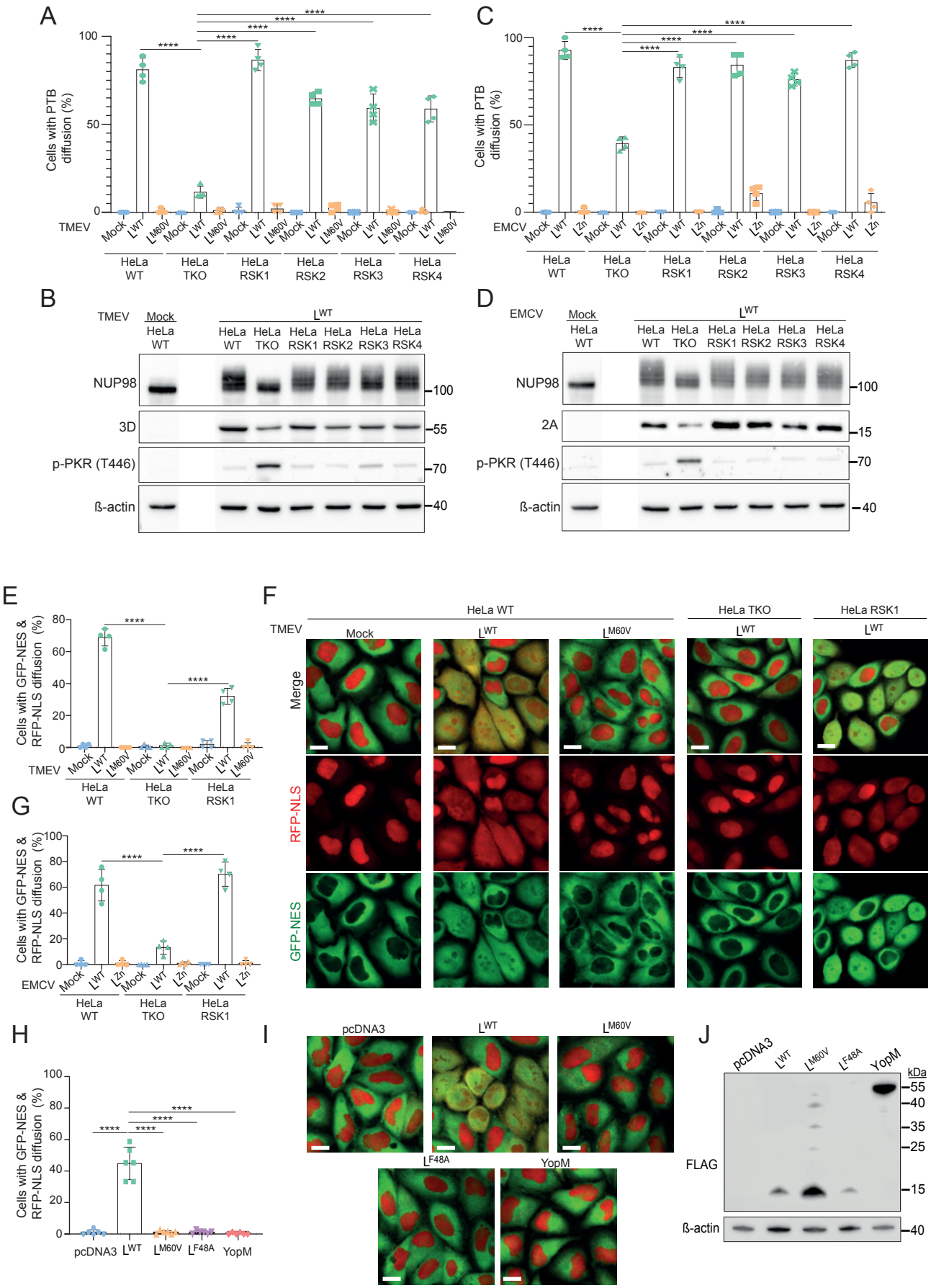
A
Cells with PTB diffusion (%)
TMEV
Mock
L^WT
L^M60V
HeLa WT
HeLa TKO
HeLa RSK1
HeLa RSK2
HeLa RSK3
HeLa RSK4
B
TMEV
Mock
HeLa WT
L^WT
NUP98
3D
p-PKR (T446)
ß-actin
100
55
70
40
C
EMCV
L^Zn
D
2A
15
E
Cells with GFP-NES & RFP-NLS diffusion (%)
F
HeLa WT
HeLa TKO
HeLa RSK1
Merge
RFP-NLS
GFP-NES
G
H
pcDNA3
L^F48A
YopM
I
J
kDa
FLAG
ß-actin

Figure 3.

A

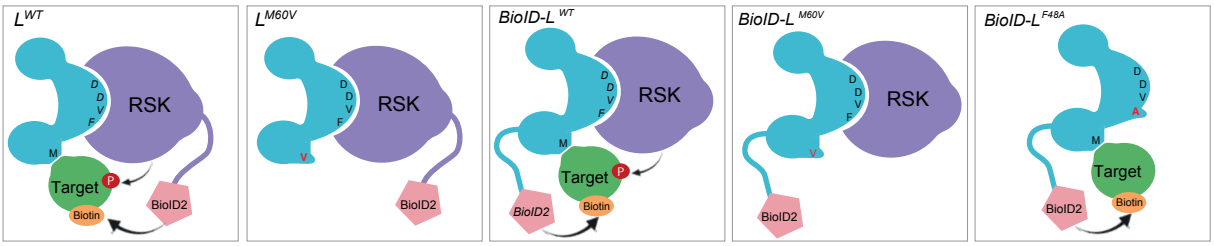

B

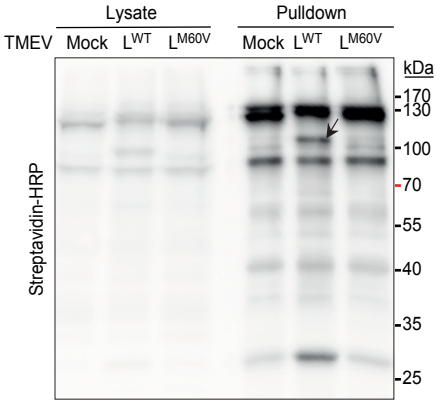

D

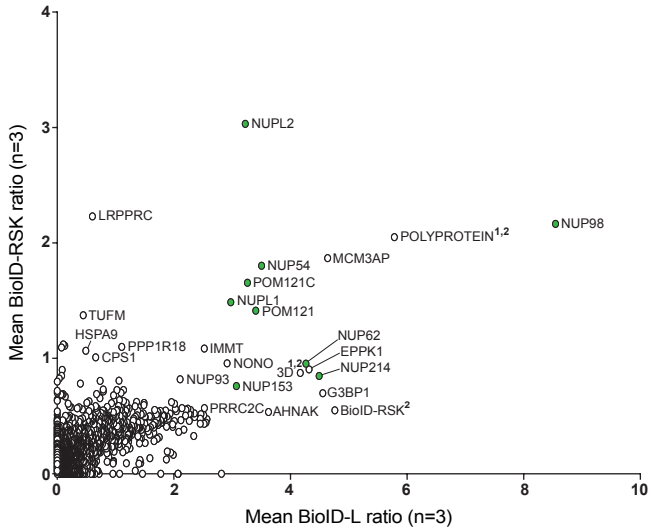

C

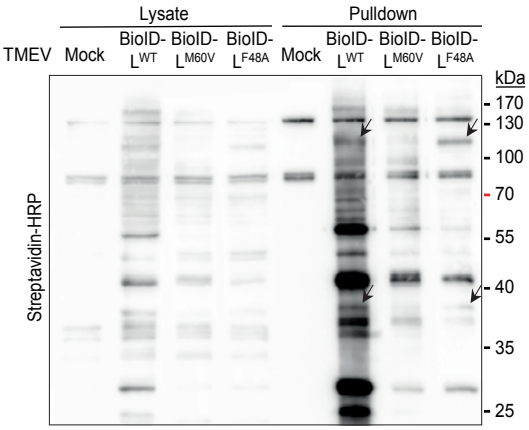

E

Ranking	BioID-RSK ratio x BioID-L ratio	Gene name	BioID-RSK ratio (mean)	BioID-L ratio (mean)	Adj. P-value BioID-RSK L^{WT} vs L^{M60V}	Adj. P-value BioID-L L^{WT} vs L^{M60V}	Adj. P-value BioID-L L^{M60V} vs L^{F48A}
1	18.51	NUP98	2.17	8.55	0.558	0.003	0.001
2	11.85	POLYPROTEIN[1,2]	2.05	5.78	NA	NA	NA
3	9.78	NUPL2	3.03	3.22	0.429	0.081	0.740
4	8.67	MCM3AP	1.87	4.64	0.614	0.003	0.001
5	6.32	NUP54	1.80	3.51	0.827	0.039	0.112
6	5.40	POM121C	1.66	3.26	0.429	0.057	0.192
7	4.81	POM121	1.41	3.40	0.827	0.032	0.085
8	4.43	NUPL1	1.49	2.98	0.614	0.015	0.007
9	4.07	NUP62	0.95	4.26	0.558	0.015	0.007
10	3.91	EPPK1	0.90	4.32	0.827	0.033	0.975
11	3.81	NUP214	0.85	4.49	0.827	0.015	0.002
12	3.64	3D[1,2]	0.87	4.17	NA	NA	NA
13	3.18	G3BP1	0.70	4.55	0.827	0.015	0.493
14	2.79	NONO	0.96	2.91	0.827	0.062	0.839
15	2.74	IMMT	1.09	2.52	0.827	0.028	0.740
16	2.62	BIOID-RSK2[2]	0.55	4.76	NA	NA	NA
17	2.34	NUP153	0.76	3.07	0.827	0.024	0.024
18	1.94	AHNAK	0.54	3.62	0.903	0.237	0.813
19	1.73	NUP93	0.82	2.11	0.827	0.081	0.493
20	1.44	PRRC2C	0.57	2.52	0.827	0.045	0.916

[1]Viral proteins
[2]Data of identified peptides belonging to shared protein groups.

F

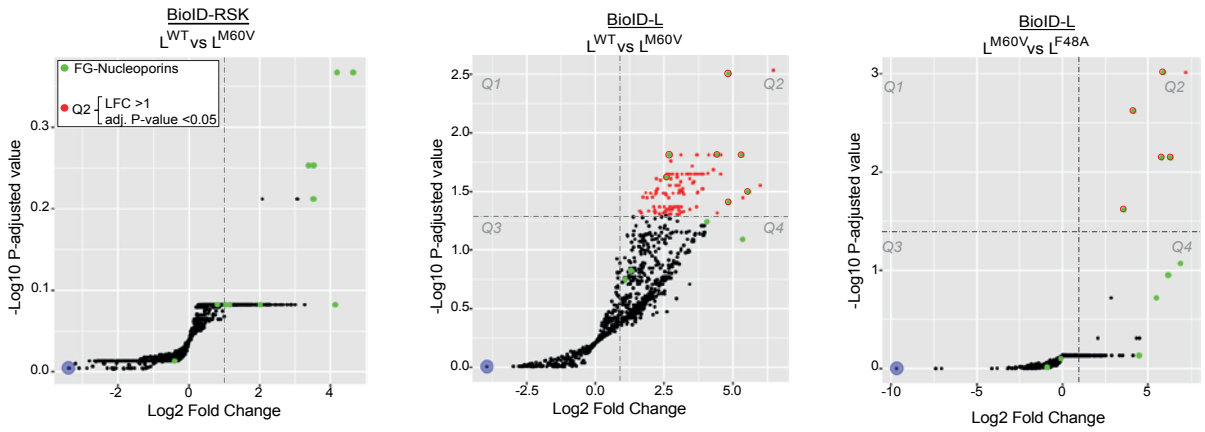

Figure 4.

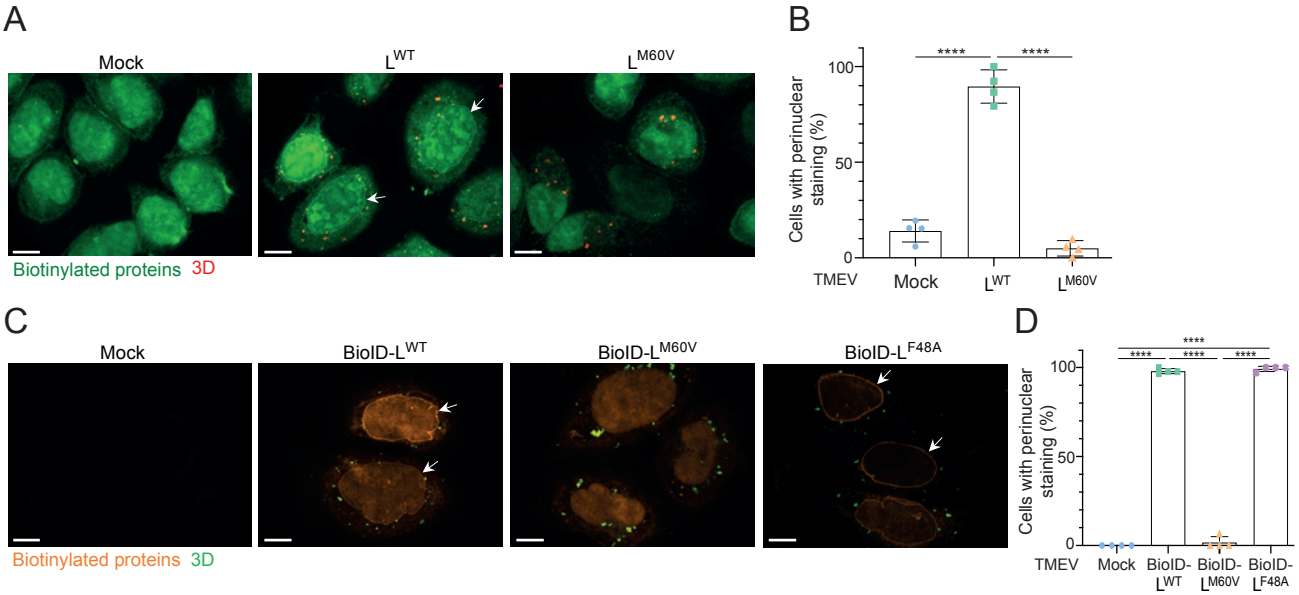
A
Mock
L^WT
L^M60V
Biotinylated proteins 3D
B
Cells with perinuclear staining (%)
100
50
0
****
****
TMEV
Mock
L^WT
L^M60V
C
Mock
BioID-L^WT
BioID-L^M60V
BioID-L^F48A
Biotinylated proteins 3D
D
Cells with perinuclear staining (%)
100
50
0
****
****
****
****
TMEV
Mock
BioID-L^WT
BioID-L^M60V
BioID-L^F48A

Figure 5.

A

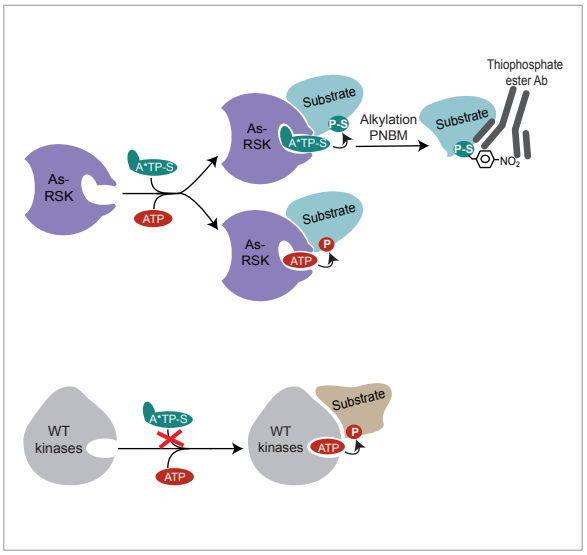

B

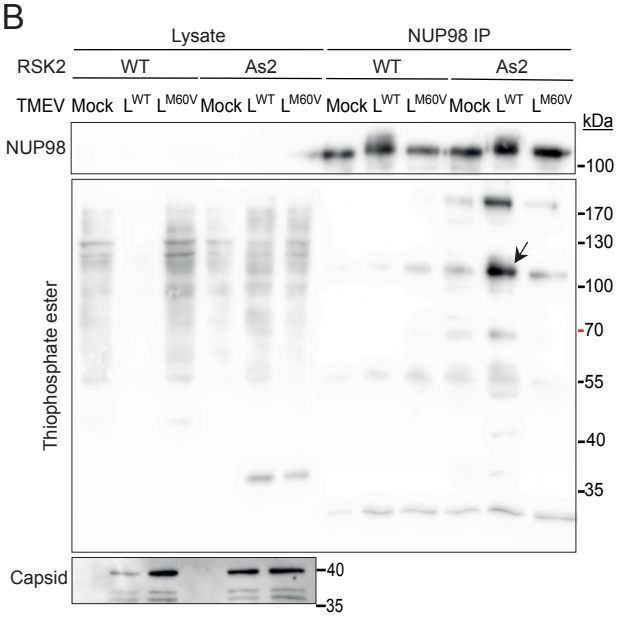

C

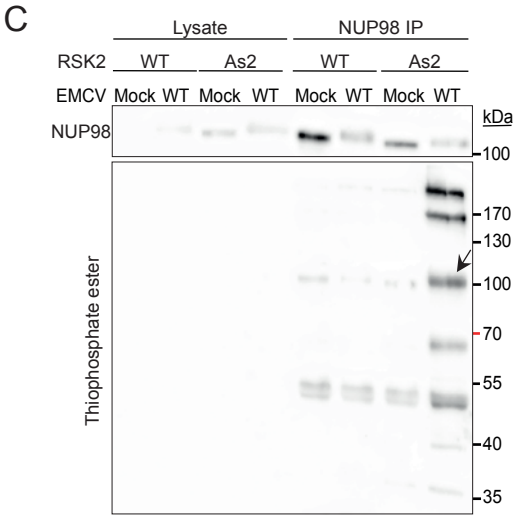
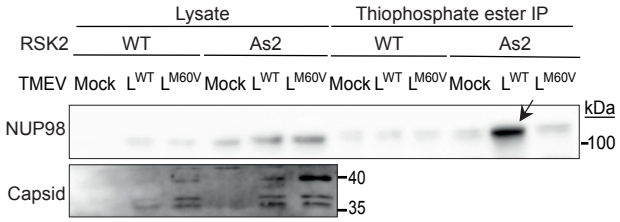
D